ACS OMEGA

http://pubs.acs.org/journal/acsodf

Article

Rapid Detection of Nonprotein Nitrogen Adulterants in Milk Powder Using Point-Scan Raman Hyperspectral Imaging Technology

Qiaoling Yang, Bing Niu, Shuqing Gu, Jinge Ma, Chaomin Zhao, Qin Chen,* Dehua Guo, Xiaojun Deng,* Yongai Yu, and Feng Zhang

Cite This: *ACS Omega* 2022, 7, 2064−2073

Read Online

ACCESS | Metrics & More | Article Recommendations

ABSTRACT: To develop a rapid detection method for nonprotein nitrogen adulterants, this experiment sets up a set of point-scan Raman hyperspectral imaging systems to qualitatively distinguish and quantitatively and positionally analyze samples spiked with a single nonprotein nitrogen adulterant and samples spiked with a mixture of nine nonprotein nitrogen adulterants at different concentrations (5×10^{-3} to 2.000%, w/w). The results showed that for samples spiked with single nonprotein nitrogen adulterants, the number of pixels corresponding to the adulterant in the region of interest increased linearly with an increase in the analyte concentration, the average coefficient of determination (R^2) was above 0.99, the minimum detection concentration of nonprotein nitrogen adulterants reached 0.010%, and the relative standard deviation (RSD) of the predicted concentration was less than 6%. For the sample spiked with a mixture of nine nonprotein nitrogen adulterants, the standard curve could be used to accurately predict the additive concentration when the additive concentration was greater than 1.200%. The detection method established in this study has good accuracy, high sensitivity, and strong stability. It provides a method for technical implementation of real-time and rapid detection of adulterants in milk powder at the port site and has good application and promotion prospects.

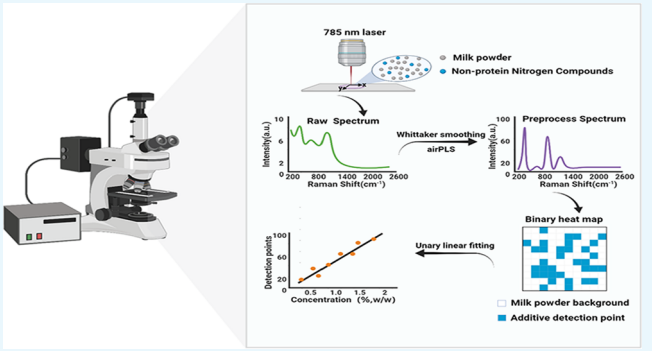

INTRODUCTION

In the field of feed processing, "nonprotein nitrogen compounds" is a general term that refers to nitrogen-containing compounds that are not proteins, including amides, free amino acids, nitrogen-containing compounds for protein degradation, and simple nitrogen-containing compounds[1] such as ammonium chloride, urea phosphate, melamine, and leucine. These compounds have a high nitrogen content and are generally colorless and odorless powders. They can be easily added to a variety of protein raw materials, such as milk powder, as an illegal additive, thereby increasing the apparent protein content.[2] Studies have shown that the long-term consumption of high nitrogen compounds such as melamine causes kidney damage and increases the risk of malignant tumors in the bladder and urethra,[3,4]as encountered in the infamous "melamine contaminated milk powder incident" in China.[5] Other nonprotein nitrogen adulterants can also harm health such as cyanuric acid is nephrotoxic[6] and thiourea leads to chronic goitrogenic and other glandular difficulties in the human.[7] At present, for nonprotein nitrogen adulterants, the detection limit of cyanuric acid in China is 25 μg/kg,[8] and the detection limit of cyanuric acid is 50 μg/kg by the relevant internal detection methods of the FDA.[9] The EU's limit value for cyromazine in milk is 0.01 mg/kg.[10] For other nonprotein nitrogen compounds in milk powder, China has not yet issued laws and regulations to establish corresponding fast and simple detection methods.

Due to the adulteration of milk powder with illegal additives, the quality and safety of dairy products has become a hot topic of public concern.[11] There are many methods of detecting illegal additives in milk powder, such as the fluorescence probe method,[12,13] colorimetry,[14,15] ultra-performance liquid chromatography/liquid chromatography-tandem mass spectrometry (UPLC/LC-MS),[16−18] nuclear magnetic resonance (NMR)[19] spectroscopy,[20−22] and electrochemical methods.[23,24] These methods are generally time-consuming and complex, and the instruments are bulky and immobile; thus, these techniques are not suitable for rapid real-time screening of large batches of samples at port sites. Spectral imaging is a

Received: October 5, 2021
Accepted: December 16, 2021
Published: January 5, 2022

rapid nondestructive testing method that combines spectroscopy, computers, digital image processing, and other technologies. The spectral characteristics and images of samples can be simultaneously assessed; thus, this technique is widely used in food,[25−28] agriculture,[29,30] biomedicine,[31,32] archeology,[33] and other fields. With regard to advantages, spectral imaging is nondestructive, highly efficient, and allows real-time monitoring of the location of additives, and thus has huge potential applications in the detection of adulteration of solid particles.[34] For example, Huang et al. used near-infrared microscopy imaging for the fast and nondestructive visual analysis of melamine in milk powder.[35] Qin et al. used point-scan Raman hyperspectral imaging combined with a self-modeling mixture analysis (SMA) to simultaneously detect ammonium sulfate, dicyandiamide, melamine, and urea in milk powder. By superimposing binary images of multiple adulterants, they obtained Raman chemical images, which were used for the identification of various adulterant particles and determination of their spatial distribution.[36]

Raman spectroscopy imaging uses Raman spectroscopy fingerprint information and two-dimensional spatial information for the accurate qualitative analysis and spatial position analysis of substances. Quantitative Raman analysis is based on the linear proportional relationship between the Raman peak intensity of the analyte and the level of analyte addition, and the calibration curve established with multiple spiking levels is used to predict the amount of analytes added. The complex composition of actual samples leads to certain challenges in quantitative analysis.

Point-scan Raman spectroscopy imaging combines Raman spectroscopy and point-scan imaging to collect the Raman data for each pixel in the given space; the molecular information is displayed in space, and the substance molecules can be analyzed qualitatively, quantitatively, and locally.[37] Compared with conventional methods, this method is easy to use, requires little sample preparation, and has high resolution; it can also identify adulterants online and display the spatial distribution of the adulterants. Herein, a point-scan Raman hyperspectral imaging instrument developed in-house is used to detect nine kinds of nonprotein nitrogen adulterants in milk powder for qualitative and quantitative analyses and is used to determine the distribution of nonprotein nitrogen adulterants in powdered milk.

RESULTS

Influence of Milk Powder Type on Adulteration Detection. A point-scan Raman hyperspectral imaging instrument was used to detect different types of milk powder, and the results are shown in Figure 1. It can be seen from Figure 1 that different types of milk powder have different Raman spectra, but they all have a common characteristic peak at 1447 cm^{-1}, which is generated by $-CH_3$ and $-CH_2$ vibration, representing the content of fat in milk powder. Then, different types of milk powder were divided into skimmed milk powder, low-fat milk powder, and whole milk powder, and mixed with thiourea adulterants, and the spectral data of the mixed samples were collected. The results are shown in Figure 2, which indicates that the Raman bands of milk powder with different fat contents have no effect on the characteristic peaks of thiourea at 475 and 730 cm^{-1} but have a greater influence on the characteristic peaks at 1093 and 1447 cm^{-1}, which explains that milk powder affects the detection of characteristic bands in the range of 1090−1500 cm^{-1}.

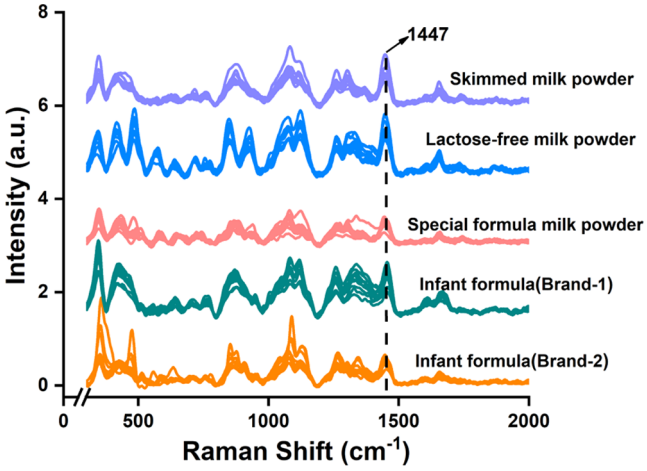

Figure 1. Raman spectra of different types of milk powder.

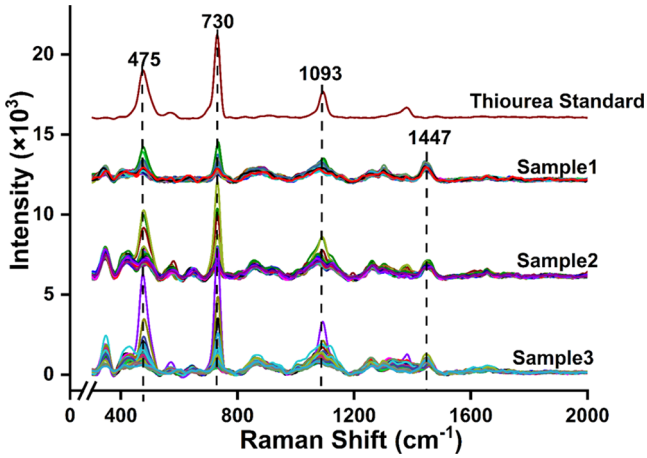

Figure 2. Raman spectra of samples with different milk powders. Sample 1, whole milk powder; sample 2, low-fat milk powder; sample 3, skimmed milk powder.

Screening Characteristic Raman Peaks of Nonprotein Nitrogen Adulterants. Using nine reference standards, such as thiourea and dicyandiamide, as samples, the Raman spectra were obtained by a single scan using a point-scan Raman spectroscopy imaging instrument; the results are shown in Figure 3. The different reference standards have different Raman shifts (Figure 3), which are mainly concentrated in the range of 500−1200 cm^{-1}. Different reference standards can be

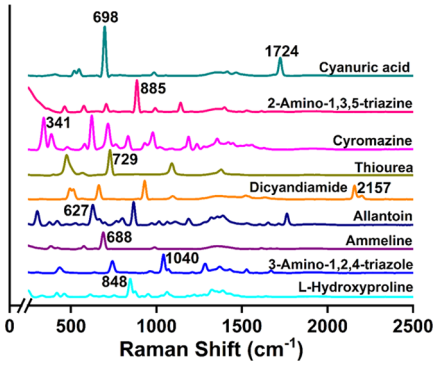

Figure 3. Raman spectra of nine nonprotein nitrogen adulterants.

https://doi.org/10.1021/acsomega.1c05533
ACS Omega 2022, 7, 2064−2073

distinguished using the characteristic Raman peaks with fingerprint information.

The characteristic Raman shifts of the nine nonprotein nitrogen samples from Figure 3 are summarized in Table 1.

Table 1. Characteristic Raman Shifts of Nine Nonprotein Nitrogen Adulterants

compound	MF	Raman shift/cm^{-1}	characteristic peak/cm^{-1}
2-amino-1,3,5-triazine	$C_3H_4N_4$	707, 885,1141	885
3-amino-1,2,4-triazole	$C_2H_4N_4$	433, 741, 1041, 1085	1040
L-hydroxyproline	$C_5H_9NO_3$	848, 1062	848
cyromazine	$C_6H_{10}N_6$	341, 622, 717, 978	341
ammeline	$C_3H_5N_5O$	688	688
cyanuric acid	$C_3H_3N_3O_3$	698, 1724	1724
thiourea	CH_4N_2S	475, 729,1090	729
allantoin	$C_4H_6O_3N_4$	303, 627, 866, 1762	627
dicyandiamide	$C_2H_4N_4$	199, 664, 930, 2157	2157

Ammeline has only one characteristic Raman shift, and the other compounds have two to four characteristic Raman shifts (Table 1). A relatively intense peak with good resolution from the other peaks is selected as the characteristic peak for each of the nine target objects, as listed in Table 1.

Rapid Visual Detection of Single Nonprotein Simulated Nitrogen Adulterants in Milk Powder. *Qualitative Analysis of Single Nonprotein Nitrogen Adulterants.* Milk powder was spiked with standard samples of each of the nine nonprotein nitrogen adulterant simulants, as shown in Table 1, at different concentrations, and the Raman hyperspectral data were collected and binarized. The results are shown in Figure 4. In the region of interest (ROI), as the additive concentration increases, the number of pixels corresponding to the adulterant (the number of detection points) increases. The minimum additive concentration that could be detected and the distribution of the adulterants can be determined by the number and location of the detection points in the heat map. When the additive concentration was 0.010%, one cyanuric acid detection point could be detected in the ROI, which shows that under the parameters of this experiment, the lowest detectable concentration of cyanuric acid in milk powder is 0.010%. In the same way, the minimum detectable concentration of 2-amino-1,3,5-triazine, thiourea, allantoin, dicyandiamide, and ammeline is 0.050%. The lowest detectable concentration of 3-amino-1,2,4-triazole, L-hydroxyproline, and cyromazine is 0.250%.

Quantitative Analysis of Samples with Single Nonprotein Nitrogen Adulteration Simulants. As shown in Figure 4, the number of pixels corresponding to the adulterant (y_1) in the ROI was counted and the average intensity of the characteristic peak (y_2) was analyzed to establish a standard curve (Table 2). As shown in Table 2, the number of pixels for the nine

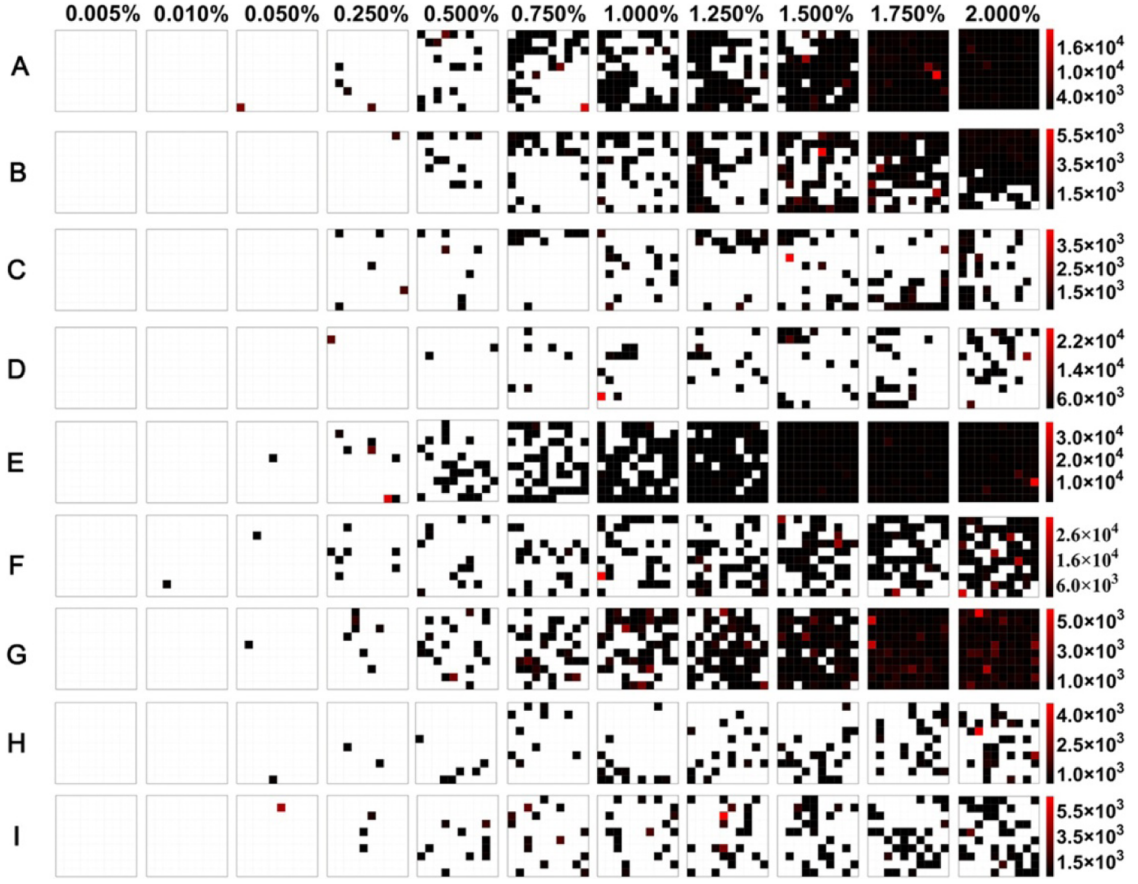

Figure 4. Binary heat map of single nonprotein simulated nitrogen adulterants (n = 3) A: 2-amino-1,3,5-triazine; B: 3-amino-1,2,4-triazole; C: L-hydroxyproline; D: cyromazine; E: ammeline; F: cyanuric acid; G: thiourea; H: allantoin; I: dicyandiamide.

https://doi.org/10.1021/acsomega.1c05533
ACS Omega 2022, 7, 2064−2073

Table 2. Standard Curve of Single Nonprotein Nitrogen Adulteration Simulants

adulterant	number of adulterant pixels (y_1)	mean intensity (y_2)
2-amino-1,3,5-triazine	$y_1 = 59.926x - 8.1849$ $R^2 = 0.9903$	$y_2 = 544.54x + 355.19$ $R^2 = 0.9049$
3-amino-1,2,4-triazole	$y_1 = 47.714x - 12.429$ $R^2 = 0.9941$	$y_2 = 58.911x + 436.99$ $R^2 = 0.2773$
L-hydroxyproline	$y_1 = 14.762x + 0.3929$ $R^2 = 0.9931$	$y_2 = 46.385x + 488.66$ $R^2 = 0.1894$
cyromazine	$y_1 = 14.381x - 4.1786$ $R^2 = 0.9907$	$y_2 = -72.395x + 2346$ $R^2 = 0.0334$
ammeline	$y_1 = 73.407x - 6.8654$ $R^2 = 0.9914$	$y_2 = 697.87x + 12.773$ $R^2 = 0.9154$
cyanuric acid	$y_1 = 34.758x - 2.8401$ $R^2 = 0.9945$	$y_2 = 558.27x + 155.76$ $R^2 = 0.9369$
thiourea	$y_1 = 59.963x - 7.5925$ $R^2 = 0.9913$	$y_2 = 402.79x + 117.44$ $R^2 = 0.9335$
allantoin	$y_1 = 15.359x - 1.3332$ $R^2 = 0.9938$	$y_2 = 117.99x + 205.28$ $R^2 = 0.9157$
dicyandiamide	$y_1 = 19.268x - 0.8198$ $R^2 = 0.9910$	$y_2 = 26.414x + 138.94$ $R^2 = 0.2114$

adulterants has a good linear relationship with the spiking concentration, and the average coefficient of determination (R^2) is greater than 0.99. However, the linearity of the relationship between the peak intensity and the spiking concentration for L-hydroxyproline, cyromazine, 3-amino-1,2,4-triazole, and dicyandiamide is poor, presumably because the sample surface is not absolutely flat, and the size of the solid particles is not completely consistent, which results in different laser scattering conditions in different pixels during the spectrum collection process; thus, the Raman signal generated is relatively unstable. In summary, the linear relationship between pixel points and concentration is selected as the quantitative basis for a single nonprotein nitrogen compound in single nonprotein nitrogen adulteration simulants.

Method Verification. To verify the accuracy of the method, three samples of milk powder spiked with single nonprotein nitrogen adulterants at different concentrations (0.60, 1.20, and 1.50%) were prepared. The Raman hyperspectral information was collected and binarized. Table 3 shows that with the addition of 0.60, 1.20, and 1.50% of the adulterants, the relative error range of the predicted concentration is −9.66 to 6.37%, and the relative standard deviation (RSD) is less than 6%, indicating that the method has high accuracy and stability and can be used to predict the concentration of additives in the milk powder.

Rapid Visual Detection of Nine Nonprotein Nitrogen Mixed Simulants in Milk Powder. *Qualitative Analysis of Nine Nonprotein Nitrogen Mixed Simulants.* Milk powder was mixed with simulants containing nine kinds of nonprotein nitrogen adulterants at concentrations (w/w) of 5×10^{-3} to 2.000%, and Raman hyperspectral information was collected. Figure 5 shows the Raman spectrum of a mixed sample containing 2.000% adulterants and milk powder. As shown in Figure 5, this method can simultaneously detect the characteristic Raman peaks of nine different additives and the characteristic peaks of milk powder (1447 cm^{-1} is generated by −CH3 and −CH2 vibration, representing the content of fat in milk powder).

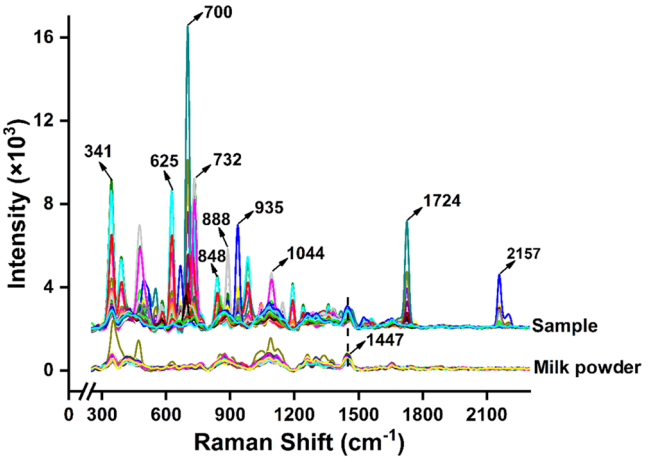

Figure 5. Raman spectra of nine nonprotein nitrogen mixed simulants (2.000%) and milk powder.

The Raman spectra of the samples with nine mixed additives at eleven concentrations were converted into corresponding binary graphs (Figure 6). It can be seen from Figure 6 that the number of pixels corresponding to the adulterants increases

Table 3. Prediction Accuracy of a Single Nonprotein Nitrogen Compound Concentration (n = 6)

compound	concentration (w/w, %)	relative error (%)	RSD (%)	compound	concentration (w/w, %)	relative error (%)	RSD (%)
2-amino-1,3,5-triazine	0.6	−4.92 to 0.64	2.20	cyanuric acid	0.6	−9.66 to −0.07	3.43
	1.2	−2.40 to 0.38	1.15		1.2	−5.38 to 3.25	2.32
	1.5	−1.90 to 2.55	1.49		1.5	−2.49 to 1.35	1.58
3-amino-1,2,4-triazole	0.6	−7.68 to −0.70	2.52	thiourea	0.6	−6.63 to 1.71	3.07
	1.2	−8.43 to −1.45	2.37		1.2	−1.89 to 0.89	1.26
	1.5	−1.60 to 1.20	1.04		1.5	−2.61 to 0.72	1.41
L-hydroxy-proline	0.6	−2.82 to 8.47	5.27	allantoin	0.6	−9.57 to 1.28	5.66
	1.2	−6.25 to 5.04	3.94		1.2	−5.96 to 4.90	3.78
	1.5	−6.94 to 2.10	3.78		1.5	−7.04 to 1.28	3.05
cyromazine	0.6	−5.22 to 6.37	5.54	dicyandiamide	0.6	−6.41 to 2.24	4.23
	1.2	−6.25 to −0.46	3.00		1.2	−1.31 to 3.02	2.04
	1.5	−6.46 to 2.81	3.86		1.5	−3.74 to 3.18	2.00
ammeline	0.6	−2.68 to 1.86	1.69				
	1.2	−1.39 to 0.88	0.93				
	1.5	−5.67 to −2.95	0.91				

https://doi.org/10.1021/acsomega.1c05533
ACS Omega 2022, 7, 2064−2073

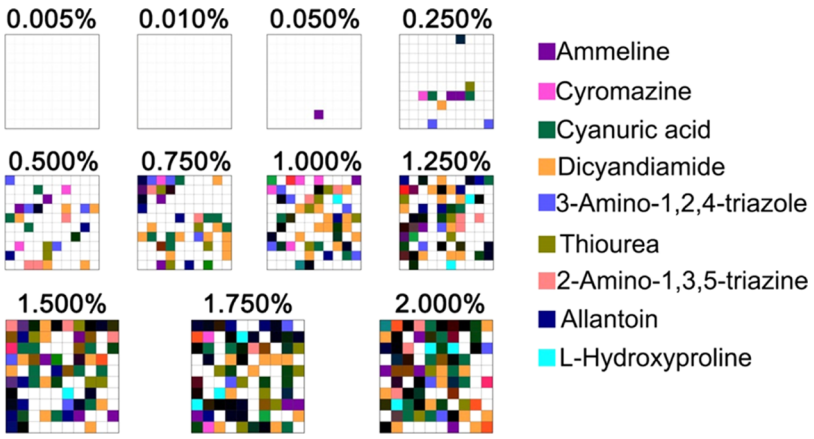

Figure 6. Binary heat map of nine nonprotein nitrogen mixed simulants (n = 3).

with increasing concentration. Based on the number of pixels for each adulterant, the minimum detection limit of each additive is not the same; for example, that of ammeline is 0.050%, and the limit of detection for cyromazine is 0.250%. Compared with the samples spiked with single nonprotein nitrogen adulteration simulants, as the types of additives in the mixed simulant increase, the lowest detectable concentration of the same additive will decrease, indicating a mutual interference from the Raman signals of the additive particles, but this effect does not affect the qualitative analysis of the nine nonprotein nitrogen adulterants.

Figures 4 and 6 illustrate that point-scanning Raman hyperspectral imaging can quickly detect large-area particles in milk powder and simultaneously furnish the spectral information and spatial information for a single additive and multiple additives in milk powder.

Quantitative Analysis of Nine Nonprotein Nitrogen Mixed Simulants. In the ROI, the number of adulterant pixels corresponding to each additive in the nine nonprotein nitrogen mixed simulants was linearly fitted to the additive concentration, and the results are shown in Table 4. There is a good linear fitting relationship between the number of pixels of the adulterants and the added concentration (R^2 > 0.99), which indicates that under these experimental conditions, the number of pixels corresponding to the adulterants can be used to predict the concentration of nonprotein nitrogen adulterants in mixed samples of milk powder containing various additives.

Table 4. Standard Curves of Nine Nonprotein Nitrogen Mixed Simulants

adulterant	linear equation	adulterant	linear equation
2-amino-1,3,5-triazine	$y = 10x - 2.5$	cyanuric acid	$y = 11.905x - 0.6429$
	$R^2 = 0.9943$		$R^2 = 0.9960$
3-amino-1,2,4-triazole	$y = 6.9524x + 0.6786$	thiourea	$y = 10.952x - 2.3214$
	$R^2 = 0.9913$		$R^2 = 0.9965$
L-hydroxyproline	$y = 6.5143x - 2.7905$	allantoin	$y = 5.5714x - 1.1071$
	$R^2 = 0.9911$		$R^2 = 0.9902$
cyromazine	$y = 6.0476x - 0.9286$	dicyandiamide	$y = 17.286x - 2.8214$
	$R^2 = 0.9910$		$R^2 = 0.9955$
ammeline	$y = 5.8138x + 0.4872$		
	$R^2 = 0.9955$		

Method Verification. Milk powder samples were spiked with three different concentrations (0.60, 1.20, and 1.50%) of nine kinds of nonprotein nitrogen adulterants, and the concentration of the additives was predicted based on the linear relationship in Table 4 (see Table 5). Table 5 shows that the relative error range and RSD of the predicted concentration become smaller as the concentration increases, which shows that the method has high accuracy and stability when the concentration of the adulterant is not less than 1.2%. This method can be used to predict the concentration of additives in milk powder, but when the adulterant concentration is low, the use of this method for quantitative analysis is not recommended because of the mutual interference of the additives.

DISCUSSION

In the field of feed processing, the reasonable addition of nonprotein nitrogen compounds can provide a nitrogen source for ruminants, but in the field of food for human consumption, nonprotein nitrogen compounds can easily be used as a source of protein adulteration, which threatens consumer health. The existing detection methods such as HPLC and colorimetry have the disadvantages of large instruments, complicated preprocessing, and time-consuming analyses, which make it difficult to achieve rapid inspection and clearance of samples at the port. In this study, we developed a point-scan Raman hyperspectral imaging system for the rapid detection of adulterants in milk powder, so as to realize the qualitative, quantitative, and positioning analysis of nine kinds of nonprotein nitrogen adulterants in milk powder. In the future, this rapid Raman hyperspectral detection method can be applied to the screening of considerable samples at ports to solve the problem of low inspection sampling efficiency.

Point-scanning Raman hyperspectral imaging was used to detect nonprotein nitrogen adulterants in milk powder. The results show that for milk powder spiked with a single nonprotein simulated adulterant, nine different nonprotein nitrogen adulterants can be accurately identified and spatially mapped. At the same time, the relationship between the number of pixels corresponding to the additive and the concentration of the additive can be used to quantitatively analyze the nonprotein nitrogen adulterants in milk powder. For samples spiked with a mixture of the nine simulated

https://doi.org/10.1021/acsomega.1c05533
ACS Omega 2022, 7, 2064−2073

Table 5. Prediction Accuracy of Nine Nonprotein Nitrogen Mixed Simulants (n = 6)

compound	concentration (w/w, %)	relative error (%)	RSD (%)	compound	concentration (w/w, %)	relative error (%)	RSD (%)
2-amino-1,3,5-triazine	0.6	−8.33 to 8.33	7.64	cyanuri- acid	0.6	−7.00 to 7.00	6.76
	1.2	−12.50 to 4.17	5.02		1.2	−11.50 to 2.50	4.98
	1.5	−3.33 to 3.33	3.33		1.5	−1.17 to 10.03	5.28
3-amino-1,2,4-triazole	0.6	−20.38 to 3.59	8.97	thiourea	0.6	−3.80 to 11.42	7.33
	1.2	−12.24 to 11.73	6.94		1.2	−6.25 to 8.97	4.33
	1.5	−10.62 to −1.03	4.88		1.5	−6.74 to 5.44	5.00
L-hydroxy-proline	0.6	−28.61 to −3.02	13.64	allantoin	0.6	−7.05 to 22.86	11.38
	1.2	−0.34 to 12.45	5.80		1.2	−8.65 to 6.30	7.32
	1.5	−10.04 to 0.19	4.98		1.5	−2.99 to 8.97	5.81
cyromazine	0.6	−19.29 to 8.27	9.91	dicyand-mide	0.6	−14.95 to 4.34	7.86
	1.2	−4.53 to 9.25	6.49		1.2	−4.44 to 0.38	2.46
	1.5	−12.60 to −1.57	5.93		1.5	−8.13 to −0.41	2.75
ammeline	0.6	−27.96 to 0.70	11.14				
	1.2	4.70 to 20.77	6.57				
	1.5	−2.38 to 9.08	5.33				

nonprotein nitrogen adulterants, this experimental method can be used to simultaneously identify the nine additives and analyze their spatial distribution. However, due to the interference between various additives and the internal milk powder, the accuracy of simultaneous quantitative analysis of nine nonprotein nitrogen adulterants is low. Therefore, it is recommended to use other methods such as dispersive solid-phase extraction-high-performance liquid chromatography-tandem mass spectrometry[1] to accurately analyze the nine nonprotein nitrogen adulterants in milk powder at the same time. Based on this result, how to improve the accuracy of technology for simultaneous detection of multiple nonprotein nitrogen compound additives is a challenge and a development direction. In short, point-scanning spectral imaging technology developed in this research can realize the qualitative, quantitative, and positional analysis of a single compound and a high concentration of multiple compounds in milk powder, and at the same time, provides a theoretical foundation for the rapid detection of other solid particles.

Compared with conventional detection technology, the point-scan Raman hyperspectral imaging system developed in this research has the following advantages: (1) The instrument is easy to transport, so this method can be operated on-site at the port. This method is green and environmentally friendly. The Raman hyperspectral imaging system avoids the pretreatment process required by conventional chromatographic and spectroscopic methods, and the measurement process is basically free of the use of harmful compounds such as organic reagents. (2) The Raman hyperspectral imaging system has a short detection time and high efficiency; the entire testing process including sample preparation can be completed within fifteen minutes, and the results are intuitively visible. High-performance liquid chromatography-mass spectrometry (HPLC-MS), including the pretreatment process, requires at least 60 min.[1] Chen et al. used line-scan Raman hyperspectral imaging to detect sodium thiocyanate in milk powder, which required 20 min.[38] (3) The method offers good accuracy and high stability. In samples spiked with single simulated nonprotein nitrogen adulterants, the concentration of nonprotein nitrogen adulterants at the added level was successfully predicted, and the RSD was less than 6%. Zhao et al.[1] used HPLC-MS to detect nonprotein nitrogen adulterants in infant formula milk powder, and the RSD ranged from 2.2 to 12.2.4. The present detection method has high sensitivity, and the detection limit is 0.01%. According to the data, in the tainted milk powder incident in 2008, the highest detected concentration of melamine was 6196.63 mg/kg, and the lowest was 1.3 mg/kg. Compared with the example, our technology can meet the range of adulteration detected in the example, and this detection limit is lower than that of the existing hyperspectral method. Qin et al.[36] used Raman spectroscopy imaging to detect adulterants in milk powder, with a minimum detection limit of 0.1%. The large particles of milk powder and complex components affect the stability and sensitivity of Raman spectroscopy; thus, the sensitivity of the Raman spectroscopy imaging system is not as good as that of chromatography and mass spectrometry. However, this detection method can meet the port's requirements for screening prohibited additives. In view of this, the rapid detection method developed in this research provides a technical platform for the real-time rapid detection of nonprotein nitrogen adulterants in bulk milk powder at the port site.

However, according to research, different adulteration technologies have a certain impact on the test results.[39] In the dry blending method, the adulterant does not change in the sample. Therefore, the main factors affecting the test results are the size of the milk powder particles and the mutual interference between various adulterants. In the wet mixing mode, the mixed sample is dissolved and solidified by freeze-drying or spray-drying. In this way, the adulterant will combine with the ingredients in the milk powder, such as lactose, fat, etc., and then recrystallize. This will reduce the concentration of adulterants and affect the test results. However, the use of wet mixing technology is more in line with the adulteration behavior of milk powder in the actual process. Therefore, the preparation of adulterated samples in the dry blend mode in this article has certain limitations, but it provides a relatively complete detection system, which can provide a theoretical basis for the rapid detection of adulterants in milk powder. In the future research process, it is necessary to consider the impact of different adulteration technologies on the detection of adulterants based on actual conditions.

CONCLUSIONS

A set of point-scan Raman hyperspectral imaging detection system was built to conduct rapid nondestructive detection of nonprotein nitrogen adulterants in milk powder. The lowest

https://doi.org/10.1021/acsomega.1c05533
ACS Omega 2022, 7, 2064−2073

detection limit for the additives was 0.01%, and the number of detection points for nine nonprotein nitrogen adulterants, such as 2-amino-1,3,5-triazine and thiourea, increased linearly with the concentration of the additive, where R^2 was greater than 0.99. For samples spiked with a single simulated nonprotein nitrogen adulterant, the relative error range of the predicted concentration of nonprotein nitrogen adulterants was −9.66 to 6.37%, and the RSD was less than 6%; thus, the method provides an accurate prediction of the concentration of additives in milk powder. The additive particles in milk powder were successfully qualitatively, quantitatively, and spatially (distribution) analyzed. The developed method requires little sample preprocessing, has a short detection period, and is thus suitable for the rapid screening of adulterants in milk powder at the port and also affords good application prospects in the actual detection of other solid particles.

EXPERIMENTAL SECTION

Samples and Reagents. The milk powder sample for analysis was obtained locally. As reagents for the assay, 2-amino-1,3,5-triazine (97.0%) and ammelin (>95.0%) were obtained from Shanghai Aladdin Biochemical Technology Co., Ltd. 3-Amino-1,2,4-triazole (≥98.0%), L-hydroxyproline (≥99.0%), thiourea (≥99.0%), and dicyandiamide (>98.0%) were obtained from ANPEL Laboratory Technologies (Shanghai) Inc. Cyromazine and cyanuric acid were obtained from TCI (Shanghai) Development Co., Ltd. Allantoin was obtained from Shanghai Macklin Biochemical Co., Ltd.

Sample Preparation. *1. Single Nonprotein Nitrogen Adulteration Simulants.* A mold made of an aluminum alloy was customized with a volume of 24 mm × 24 mm × 2 mm; the size of the sample holding tank was 24 mm × 24 mm × 1 mm, as shown in Figure 7a. Before preparing the sample, the

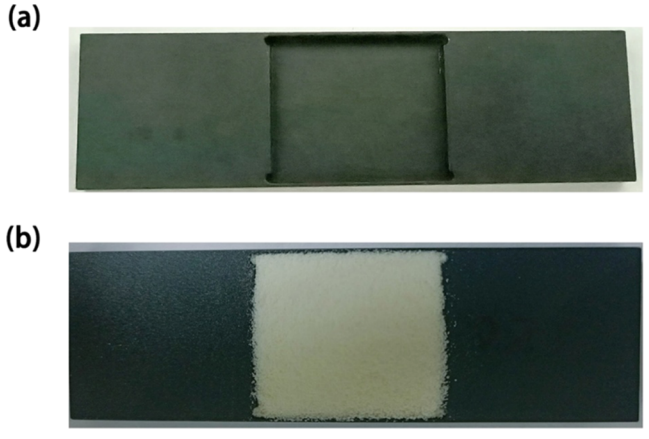

Figure 7. Inspection mold (a) and mixed sample diagram (b).

nonprotein nitrogen compound and milk powder were ground for 2 min, and nine nonprotein nitrogen adulterants were mixed into the milk powder to prepare mixtures at eleven concentration levels for each adulterant (w/w): 5×10^{-3}, 1.0×10^{-2}, 5.0×10^{-2}, 2.50×10^{-1}, 5.00×10^{-1}, 7.50×10^{-1}, 1.000, 1.250, 1.500, 1.750, and 2.000%. These single nonprotein nitrogen adulteration simulants with a total mass of 1 g were placed in 5 mL polypropylene centrifuge tubes. A vortex mixer was used to shake and spin the tubes to ensure a uniform distribution of the adulterant particles in the dry milk. In the experiment, the dry milk samples were spiked with single nonprotein nitrogen adulteration simulants at ninety-nine different spiking levels.

2. Mixture of Nine Nonprotein Nitrogen Adulterant Simulants. The nine nonprotein nitrogen adulterants at the same concentration were ground with milk powder for 2 min and then added to a 5 ml centrifuge tube. A vortex mixer was used to shake and spin the tubes to obtain the sample spiked with the mixture of nine nonprotein nitrogen adulterant simulants. The sample was collected on an electric loading platform to obtain the hyperspectral image information in the ROI. For collection of the hyperspectral information, each sample was divided into three equal parts for imaging in triplicate. To reduce errors, attempts were made to keep the sample surface flat.

Point-Scan Raman Hyperspectral Imaging System. The main components of the hardware system are a high-precision positioning and scanning device, an optical microscope platform, and a Raman spectrometer module (Figure 8). The high-precision positioning and scanning device consists of two parts: one is a two-dimensional microarea positioning electric platform with a positioning accuracy better than 5 μm and the other is an electric focusing platform with a minimum step length of 0.1 μm. The optical microscope uses an infinity correction objective lens, which is convenient for inserting the Raman spectrometer module in the optical path of the microscope. The Raman spectrometer module is combined with the microscope optical path through a beam splitter, and the parallel beams emitted by the Raman probe are reflected by the beam splitter and then focused on the sample by the microscope objective lens. The laser spot and imaging information for the sample can be observed using a CMOS camera. The excitation wavelength of the point laser was 785 nm, the maximum output power was 600 mW, and the spectral width was 0.076 nm. The corresponding Raman imaging spectrometer has a collection range of 200−3200 cm^{-1} and a spectral resolution of 0.7 nm. The maximum speed of the electric translation platform is 20 mm/s, the positioning accuracy is ≤±5 μm, and the minimum step size is 0.1 μm. The resolution of the CMOS camera is 2048 × 1536 pixels, and the size of the collected pixels is 3.2 μm × 3.2 μm.

The translation step length of the electric translation stage, the position of the microspot, the Raman hyperspectral acquisition parameters, and the preprocessing method applied to the spectral data can be adjusted through a software control system. When collecting hyperspectral information, the point laser is reflected on the surface of the sample using a dichroic beam splitter. The CMOS camera and spectrometer collect the image and Raman spectral data of the corresponding point. As the electric translation stage moves along the *X*- and *Y*-axis, the entire sample is scanned. During the experiment, the focus was controlled by adjusting the coarse and fine collimation spirals. When the laser spot is in the center of the image and is bright and without ghosting, the focus is completed.

The process of collecting the sample's Raman hyperspectral data by the point-scan Raman hyperspectral imaging system is as follows: (1) Put the sample into the mold, then gently flatten its surface with a glass sheet, and put it into the testing table. (2) Open the software system, and adjust the collection parameters and spectrum processing mode. (3) Click "continuous collection". Adjust the starting position of the laser and the size of the spot. (4) Set the size of the collection area and the number of pixels, click "start scan collection".

https://doi.org/10.1021/acsomega.1c05533
ACS Omega 2022, 7, 2064−2073

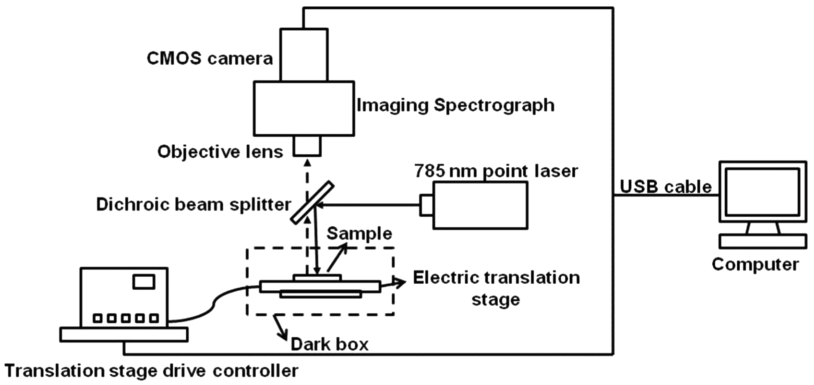

Figure 8. Schematic diagram of the point-scan Raman hyperspectral imaging system.

With the movement of the loading platform, the scan of the entire sample is finally completed. The instrument acquisition parameters used in the experiment were as follows: a laser power of 300 mw, the integration time of 1000 ms, and the acquisition area of 24 mm × 24 mm and 10 × 10 pixels. Herein, the acquisition time required to complete a quality score sample was approximately 6 min.

Analysis of Hyperspectral Data. The point-scan Raman hyperspectral imaging system collects 3D data containing 2048 bands. To reduce the computational complexity for processing the hyperspectral data, the dimensionality of the data must be reduced prior to data analysis. Data processing was performed as follows:

(1) Collection of Single Spectrum Effective Data. Nine-hundred and twenty-one effective bands (330−2199 cm^{-1}) were extracted from 2048 bands for processing. Uspectral-Plus5.1.0 software was used for band selection.

(2) Removal of the Noise Signal and Fluorescence Background. The Whittaker smoothing method and adaptive iteratively reweighted penalized least squares (airPLS) in the software system were used to eliminate background random noise signals and fluorescence background interference.

(3) Identification of Peaks. All of the Raman spectrum data were extracted from the characteristic peaks of nine kinds of nonprotein nitrogen adulterants, and the data were rearranged in a 10 × 10 matrix according to the collection direction of the samples in the region of interest.

(4) Assembling and Visualizing Spatial Multidimensional Spectra. The maximum Raman intensity of the milk powder background at the peak temperature for the nonprotein nitrogen adulterants was set as the threshold. Pixels for which the Raman intensity was higher than the threshold were judged as adulterated particles and were displayed in different colors in the binary image, which was lower than the threshold. The milk powder background was set to be displayed in white so that a binary image of the sample in the ROI was obtained. The binary image clearly showed the detection and spatial distribution of the adulterated particles. The single-band image binarization process was performed using Prism 8.0 software (GraphPad Software).

(5) Superposition of the Binary Heat Maps. At the same concentration, the binary heat maps of a single nonprotein nitrogen-adulterated mixture were superimposed to obtain the binary heat maps of nine nonprotein nitrogen mixed simulants. The image superposition process was carried out using the software Photoshop CS6 (Adobe).

AUTHOR INFORMATION

Corresponding Authors

Qin Chen − *School of Life Sciences, Shanghai University, Shanghai 200444, P. R. China*; Email: chenqincc@shu.edu.cn

Xiaojun Deng − *Technical Center for Animal, Plant and Food Inspection and Quarantine, Shanghai Customs, Shanghai 200135, P. R. China*; orcid.org/0000-0002-1051-2507; Email: xjdeng@yeah.net

Authors

Qiaoling Yang − *School of Environmental and Chemical Engineering, Shanghai University, Shanghai 200444, P. R. China; School of Life Sciences, Shanghai University, Shanghai 200444, P. R. China*; orcid.org/0000-0002-0858-7745

Bing Niu − *School of Life Sciences, Shanghai University, Shanghai 200444, P. R. China*

Shuqing Gu − *Technical Center for Animal, Plant and Food Inspection and Quarantine, Shanghai Customs, Shanghai 200135, P. R. China*

Jinge Ma − *Technical Center for Animal, Plant and Food Inspection and Quarantine, Shanghai Customs, Shanghai 200135, P. R. China*

Chaomin Zhao − *Technical Center for Animal, Plant and Food Inspection and Quarantine, Shanghai Customs, Shanghai 200135, P. R. China*

Dehua Guo − *Technical Center for Animal, Plant and Food Inspection and Quarantine, Shanghai Customs, Shanghai 200135, P. R. China*

Yongai Yu − *Shanghai Oceanhood opto-electronics tech Co., LTD., Shanghai 201201, P. R. China*

Feng Zhang − *Chinese Academy of Inspection and Quarantine, Beijing 100176, P. R. China*; orcid.org/0000-0002-7888-9669

Complete contact information is available at: https://pubs.acs.org/10.1021/acsomega.1c05533

Author Contributions

Q.Y. planned, executed the experiments, and wrote the manuscript; B.N. edited the paper; S.G., J.M., and C.Z. are scientific advisors; Q.C. is a scientific advisor and edited the paper; D.G. and X.D. provided the laboratory facilities; Y.Y. provided a spectrometer; and F.Z. provided some literature resources.

Notes

The authors declare no competing financial interest.

https://doi.org/10.1021/acsomega.1c05533
ACS Omega 2022, 7, 2064−2073

■ ACKNOWLEDGMENTS

The authors are grateful for support given by the National Key Research and Development Plan Project (2018YFC1603503), Shanghai Agricultural Research Project (19391901500), Science and Technology Joint Project of the Yangtze River Delta (19395810100), and Shanghai Technical Standard Project (18DZ2201200).

■ ABBREVIATIONS USED

ROI, region of interest; UPLC/LC-MS, ultra-performance liquid chromatography/liquid chromatography-tandem mass spectrometry; NMR, nuclear magnetic resonance; SMA, self-modeling mixture analysis; RSD, relative standard deviation; airPLS, adaptive iteratively reweighted penalized least squares; HPLC-MS, high-performance liquid chromatography-mass spectrometry

■ REFERENCES

(1) Zhao, S.; Xionghai, Y. I.; Cheng, J.; Pan, X. B.; Guo, D. H.; Zhu, J.; Deng, X. J. Determination of 19 Kinds of Nonprotein Nitrogen Compounds in Powdered Formulas by Dispersive Solid Phase Extraction-High Performance Liquid Chromatography-Tandem Mass Spectrometry. *Chin. J. Anal. Chem.* **2016**, *44*, 1227−1235.

(2) Shellaiah, M.; Sun, K. W. Review on nanomaterial-based melamine detection. *Chemosensors* **2019**, *7*, 9.

(3) Liu, J.-D.; Liu, J.-J.; Yuan, J.-H.; Tao, G.-H.; Wu, D.-S.; Yang, X.-F.; Yang, L.-Q.; Huang, H.-Y.; Zhou, L.; Xu, X.-Y.; Hu, J.-J.; Zhuang, Z.-X. Proteome of melamine urinary bladder stones and implication for stone formation. *Toxicol. Lett.* **2012**, *212*, 307−314.

(4) Wu, Y. N.; Zhang, Y. Analytical chemistry, toxicology, epidemiology and health impact assessment of melamine in infant formula: Recent progress and developments. *Food Chem. Toxicol.* **2013**, *56*, 325−335.

(5) Gossner Céline, M.-E.; Schlundt, J.; Ben Embarek, P.; Hird, S.; Lo-Fo-Wong, D.; Beltran Jose Javier, O.; Teoh Keng, N.; Tritscher, A. The Melamine Incident: Implications for International Food and Feed Safety. *Environ. Health Perspect.* **2009**, *117*, 1803−1808.

(6) Von Tungeln, L. S.; Jacob, C. C.; Olson, G. R.; da Costa, G.; Beland, F. A. Effect of urinary pH upon the renal toxicity of melamine and cyanuric acid. *J. Environ. Sci. Health, Part C: Toxicol. Carcinog.* **2021**, *39*, 340−355.

(7) Arab Chamjangali, M.; Goudarzi, N.; Ghochani Moghadam, A.; Amin, A. H. An on-line spectrophotometric determination of trace amounts of thiourea in tap water, orange juice, and orange peel samples using multi-channel flow injection analysis. *Spectrochim. Acta, Part A* **2015**, *149*, 580−587.

(8) SN/T, Determination of Melamine and Cyanuric Acid in Foodstuffs for Export-HPLC-MS /MS Method. General Administration of Quality Supervision, Inspection and Quarantine of the People's Republic of China, 2011, *SN/T 3032-2011*.

(9) FDA, Laboratory Information Bulletin (LIB) 4422: Melamine and Cyanuric Acid Residues In Foods. The USA, 2008, Vol. *4422*.

(10) EU, amending Annexes II and III to Regulation (EC) No 396/2005 of the European Parliament and of the Council as regards maximum residue levels for cyromazine, fenpropidin, formetanate, oxamyl and tebuconazole in or on certain products, 2014, Vol. *61*.

(11) Xiao, G.; Qin, C.; Wenju, Z.; Qin, C. Development of a real-time quantitative PCR assay using a TaqMan minor groove binder probe for the detection of α-lactalbumin in food. *J. Dairy Sci.* **2016**, *99*, 1716−1724.

(12) Lin, C.; Zhong, C.; Song, Y.; Wang, L. Ratiometric fluorescence detection of melamine in milk by a zirconium-based metal-organic frameworks composite. *Microchem. J.* **2021**, *162*, No. 105837.

(13) Lei, C.H.; Zhao, X.E.; Jiao, S.L.; He, L.; Li, Y.; Zhu, S.Y.; You, J.M. A turn-on fluorescent sensor for the detection of melamine based on the anti-quenching ability of Hg 2+ to carbon nanodots. *Anal. Methods* **2016**, *8*, 4438−4444.

(14) Inamuddin; Kanchi, S. One-pot biosynthesis of silver nanoparticle using Colocasia esculenta extract: Colorimetric detection of melamine in biological samples. *J. Photochem. Photobiol., A* **2020**, 391.

(15) Liu, S.; Kannegulla, A.; Kong, X.; Sun, R.; Liu, Y.; Wang, R.; Yu, Q.; Wang, A. X. Simultaneous colorimetric and surface-enhanced Raman scattering detection of melamine from milk. *Spectrochim. Acta, Part A* **2020**, *231*, No. 118130.

(16) Ge, X.; Wu, X.; Liang, S.; Su, M.; Sun, H. Trace residue analysis of dicyandiamide, cyromazine, and melamine in animal tissue foods by ultra-performance liquid chromatography. *J. Food Drug Anal.* **2016**, *24*, 579−585.

(17) Shen, Y.; Han, C.; Zhou, X.; Chen, X.; Huang, F.; Zhu, Z. Microwave-assisted extraction and determination of dicyandiamide residue in infant formula samples by liquid chromatography-tandem mass spectrometry. *J. Dairy Sci.* **2013**, *96*, 6877−6882.

(18) Ge, X. S.; Wu, X. Q.; Wang, J. M.; Liang, S. X.; Sun, H. W. Highly sensitive determination of cyromazine, melamine, and their metabolites in milk by molecularly imprinted solid-phase extraction combined with ultra-performance liquid chromatography. *J. Dairy Sci.* **2015**, *98*, 2161−2171.

(19) Li, Q.; Meng, X.; Zhu, D.; Pang, X.; Wang, K.; Frew, R.; Chen, G. Determination of Nonprotein Nitrogen Components of Milk by Nuclear Magnetic Resonance. *Anal. Lett.* **2016**, *49*, 2953−2963.

(20) Liang, W.; Zhu, Z.; Yang, B.; Zhu, X.; Guo, W. Detecting melamine-adulterated raw milk by using near-infrared transmission spectroscopy. *J. Food Process Eng.* **2021**, *44*, No. e13685.

(21) Dhakal, S.; Chao, K.; Qin, J.; Kim, M. S. In *Raman-Spectroscopy-Based Chemical Contaminant Detection in Milk Powder, Sensing for Agriculture And Food Quality And Safety Vii, Baltimore, Maryland, United States*; Kim, M. S.; Chao, K.; Chin, B. A., Eds.; Baltimore: Maryland, United States, 2015.

(22) Jawaid, S.; Talpur, F. N.; Sherazi, S.; Nizamani, S. M.; Khaskheli, A. A. Rapid detection of melamine adulteration in dairy milk by SB-ATR−Fourier transform infrared spectroscopy. *Food Chem.* **2013**, *141*, 3066−3071.

(23) Regasa, M. B.; Refera Soreta, T.; Femi, O. E.; C Ramamurthy, P. Development of molecularly imprinted conducting polymer composite film-based electrochemical sensor for melamine detection in infant formula. *ACS Omega* **2020**, *5*, 4090−4099.

(24) Liao, C.-W.; Chen, Y.-R.; Chang, J.-L.; Zen, J.-M. Single-run electrochemical determination of melamine in dairy products and pet foods. *J. Agric. Food Chem.* **2011**, *59*, 9782−9787.

(25) Yu, H. D.; Qing, L. W.; Yan, D. T.; Xia, G. H.; Zhang, C. H.; Yun, Y. H.; Zhang, W. M. Hyperspectral imaging in combination with data fusion for rapid evaluation of tilapia fillet freshness. *Food Chem.* **2021**, *348*, No. 129129.

(26) Ouyang, Q.; Wang, L.; Park, B.; Kang, R.; Chen, Q. Simultaneous quantification of chemical constituents in matcha with visible-near infrared hyperspectral imaging technology. *Food Chem.* **2021**, *350*, No. 129141.

(27) Caporaso, N.; Whitworth, M. B.; Fisk, I. D. Total lipid prediction in single intact cocoa beans by hyperspectral chemical imaging. *Food Chem.* **2021**, *344*, No. 128663.

(28) Khamsopha, D.; Woranitta, S.; Teerachaichayut, S. Utilizing near infrared hyperspectral imaging for quantitatively predicting adulteration in tapioca starch. *Food Control* **2021**, *123*, No. 128663.

(29) Li, T.; Zhu, Z.; Cui, J.; Chen, J.; Shi, X.; Zhao, X.; Jiang, M.; Zhang, Y.; Wang, W.; Wang, H. Monitoring of leaf nitrogen content of winter wheat using multi-angle hyperspectral data. *Int. J. Remote Sens.* **2021**, *42*, 4672−4692.

(30) Su, W. H.; Yang, C.; Dong, Y. H.; Johnson, R.; Page, R.; Szinyei, T.; Hirsch, C. D.; Steffenson, B. J. Hyperspectral imaging and improved feature variable selection for automated determination of deoxynivalenol in various genetic lines of barley kernels for resistance screening. *Food Chem.* **2021**, *343*, No. 128507.

(31) Kujdowicz, M.; Placha, W.; Mech, B.; Chrabaszcz, K.; Okon, K.; Malek, K. In Vitro Spectroscopy-Based Profiling of Urothelial

https://doi.org/10.1021/acsomega.1c05533
ACS Omega 2022, 7, 2064−2073

Carcinoma: A Fourier Transform Infrared and Raman Imaging Study. *Cancers* **2021**, *13*, No. 123.
(32) Wang, C.; Yu, H.; Yao, W.-r.; Cheng, Y.-l.; Guo, Y.-h.; He, Q.; Tan, Z.-q.; Xie, Y.-f. A Study on the Screening of Anti-Inflammatory Drug Diclofenac Sodium in Dietary Supplements by Near Infrared Hyperspectral Imaging. *Spectrosc. Spectral Anal.* **2021**, *41*, 592−598.
(33) Cucci, C.; Picollo, M.; Chiarantini, L.; Uda, G.; Fiori, L.; De Nigris, B.; Osanna, M. Remote-sensing hyperspectral imaging for applications in archaeological areas: Non-invasive investigations on wall paintings and on mural inscriptions in the Pompeii site. *Microchem J.* **2020**, *158*, No. 105082.
(34) Yaseen, T.; Sun, D.-W.; Cheng, J.-H. Raman imaging for food quality and safety evaluation: Fundamentals and applications. *Trends Food Sci. Technol.* **2017**, *62*, 177−189.
(35) Huang, Y.; Min, S.; Duan, J.; Wu, L.; Li, Q. Identification of additive components in powdered milk by NIR imaging methods. *Food Chem.* **2014**, *145*, 278−283.
(36) Qin, J.; Chao, K.; Kim, M. S. Simultaneous detection of multiple adulterants in dry milk using macro-scale Raman chemical imaging. *Food Chem.* **2013**, *138*, 998−1007.
(37) Dhakal, S.; Chao, K.; Qin, J.; Kim, M.; Chan, D. Raman spectral imaging for quantitative contaminant evaluation in skim milk powder. *J. Food Meas.Charact.* **2016**, *10*, 374−386.
(38) Liu, C.; Yang, J. Y.; Wang, Q. Y.; Huang, W. Q.; Wang, C. P.; Wang, X. B.; Chen, L. P. Non-Invasive Detection of Sodium Thiocyanate in Milk Powder Using Line-Scanning Raman Hyperspectral Imaging System. *Food Sci.* **2018**, *39*, 295−300.
(39) Scholl, P. F.; Bergana, M. M.; Yakes, B. J.; Xie, Z.; Zbylut, S.; Downey, G.; Mossoba, M.; Jablonski, J.; Magaletta, R.; Holroyd, S. E.; Buehler, M.; Qin, J.; Hurst, W.; LaPointe, J. H.; Roberts, D.; Zrybko, C.; Mackey, A.; Holton, J. D.; Israelson, G. A.; Payne, A.; Kim, M. S.; Chao, K.; Moore, J. C. Effects of the Adulteration Technique on the Near-Infrared Detection of Melamine in Milk Powder. *J. Agric. Food Chem.* **2017**, *65*, 5799−5809.

https://doi.org/10.1021/acsomega.1c05533
ACS Omega 2022, 7, 2064−2073